THE UNIVERSITY of EDINBURGH

Edinburgh Research Explorer

Automated search for galactic star clusters in large multiband surveys

OPEN ACCESS

arXiv:0709.1275v2 [astro-ph] 9 May 2008

Automated search for galactic star clusters in large multiband surveys: I. Discovery of 15 new open clusters in the Galactic anticenter region

S.E. Koposov[1,2,3], E.V. Glushkova[2] and I.Yu. Zolotukhin[2]

[1] Max Planck Institute for Astronomy, Königstuhl 17, D-69117, Heidelberg, Germany
[2] Sternberg Astronomical Institute, Universitetskiy pr. 13, 119992 Moscow, Russia
[3] Institute of Astronomy, University of Cambridge, Madingley Road, Cambridge CB3 0HA, UK
  S. Koposov e-mail: `koposov@mpia.de`, E. Glushkova e-mail: `elena@sai.msu.ru`

ABSTRACT

Aims. According to some estimations, there are as many as 100000 open clusters in the Galaxy, but less than 2000 of them have been discovered, measured, and cataloged. We plan to undertake data mining of multiwavelength surveys to find new star clusters.
Methods. We have developed a new method to search automatically for star clusters in very large stellar catalogs, which is based on convolution with density functions. We have applied this method to a subset of the Two Micron All Sky Survey catalog toward the Galactic anticenter.
We also developed a method to verify whether detected stellar groups are real star clusters, which tests whether the stars that form the spatial density peak also fall onto a single isochrone in the color-magnitude diagram. By fitting an isochrone to the data, we estimate at the same time the main physical parameters of a cluster: age, distance, color excess.
Results. For the present paper, we carried out a detailed analysis of 88 overdensity peaks detected in a field of 16×16 degrees near the Galactic anticenter. From this analysis, 15 overdensities were confirmed to be new open clusters and the physical and structural parameters were determined for 12 of them; 10 of them were previously suspected to be open clusters by Kronberger (2006) and Froebrich (2007). The properties were also determined for 13 yet-unstudied known open clusters, thus almost tripling the sample of open clusters with studied parameters in the anticenter. The parameters determined with this method showed a good agreement with published data for a set of well-known clusters.

Key words. Galaxy: structure - open clusters and associations:general - Surveys - Catalogs

1. Introduction

Star clusters are unique laboratories for investigation of a wide range of astrophysical problems relating to star formation, stellar evolution, the formation and structure of the Milky Way, and the distance scale of the Universe. As star clusters are usually single-age and single-metallicity populations, distance, age, and reddening in the cluster's direction can be determined with much higher accuracy than for isolated, or "field", stars. To define at least a reliable ranking of the open cluster properties, we need a large sample of objects whose age, distance, and metallicity are accurately and homogeneously known. So far, 1756 open clusters were cataloged (Dias et al., 2002), but the basic physical parameters are known for less than 700 objects. And, all these parameters were derived by different authors based on heterogeneous observational data. Most of the open clusters in the Galaxy are probably not yet found because open clusters are concentrated near the Galactic plane where extinction by interstellar dust is most severe. Some literature estimates put the total number of open clusters in the Galaxy at 10^5 (see, for example Surdin, 2000). Modern all-sky surveys (e.g., Two Micron All Sky Survey (2MASS), Deep Near Infrared Survey of the Southern Sky (DENIS), Sloan Digital Sky Survey(SDSS), etc.) provide a large store of information to study open clusters com-

prehensively and homogeneously. Near-infrared surveys are especially useful because the data are far less affected by high reddening in the Galactic plane where the most open clusters are located.

Numerous attempts were made in recent years to search for star clusters using such large surveys. However, the total number of newly-discovered clusters with robust determinations of their physical parameters does not exceed two dozen. Dutra et al. (2003) performed a visual search for IR clusters and similar objects in the direction of known nebulae using the 2MASS Atlas and found 179 embedded clusters and stellar groups. However, it proved impossible to find the physical parameters of this type of objects through isochrone fitting. Ivanov et al. (2002) and Borissova et al. (2003) found 11 peaks by automated algorithm and 3 peaks by visual inspection in the apparent stellar surface density in the 2MASS point source catalog. They detected mostly embedded IR clusters, so the physical parameters could be derived only for one object. Drake (2005) performed an automated search for clusters in the United States Naval Observatory (USNO) A2 catalog using the method developed by Ivanov et al. (2002) and found 8 new candidates. However, their basic parameters were not derived. Kronberger et al. (2006) visually inspected Digitized Sky Survey (DSS) and 2MASS images and selected 66 candidate clusters. For 9 of 24 of the most probable clusters within this sample, the authors determined fundamental parameters by isochrone fitting. Froebrich et al. (2007) used star

density maps obtained from 2MASS and found 1021 new cluster candidates. The authors statistically evaluated the contamination of their sample to be of about 50% and left verification of the nature of each individual cluster for future investigations.

We developed a new efficient method of searching stellar catalogs for star clusters of different radii based on the convolution of the cataloged stellar source density maps with Gaussians (a similar method was used to search for dwarf Spheroidal galaxies and globular clusters in SDSS; Koposov et al., 2007, 2008). The method automatically finds cluster candidates and then confirms them by testing whether the spatially clustered, potential cluster members lie on the same isochrone in the color-magnitude diagram. At the same time, this procedure determines the basic cluster parameters (age, radius, distance, and color excess) by fitting the isochrone position. Below, we describe our method of automatic search for stellar overdensities and the results of its application to the 2MASS data in the field of 16×16 degrees in the region of the Galactic anticenter.

2. Method of automated search for star clusters

This work aims to provide a fast, simple, and efficient method of identifying open clusters in very large photometric catalogs, such as 2MASS, SDSS, DENIS etc. The overall density of the stars in the Milky Way (MW) is high at low latitudes and can vary rapidly because of dust, etc. So, it is not easy to find star clusters algorithmically on such a complex background. Even when a peak is found, it is important to check whether the candidate is indeed an evolutionarily connected group of cluster members or merely a group of stars clustered by chance.

Therefore, the method must be capable of detecting density peaks on a sharply changing background and to evaluate their statistical significance. To develop a universal technique for all data sources, we have to make it independent of any pixelization effects and thus applicable to star structures of any size. To ensure this, we built a density map, which presents the number of counts in (RA, Dec) coordinates. Then, we convolved this image with a special filter demonstrated in Fig. 1. The filter curve is the difference between two 2-D Gaussian profiles and has zero integral. Employing this special shape of filter, we ensure that a flat, or even slowly changing background produces a zero signal, whereas the concentrations of stars exhibit a high signal. The family of such filters called Difference of Gaussians are well studied and used in computer vision science for feature detection at various scales (Babaud et al., 1986; Lindenberg, 1998). The convolution with this filter is equivalent to the subtraction of the density maps convolved with the gaussians of different widths. The density map convolved with the small Gaussian is used to detect the small scale overdensities, while the density map convolved with wider Gaussian is the estimation of local background.
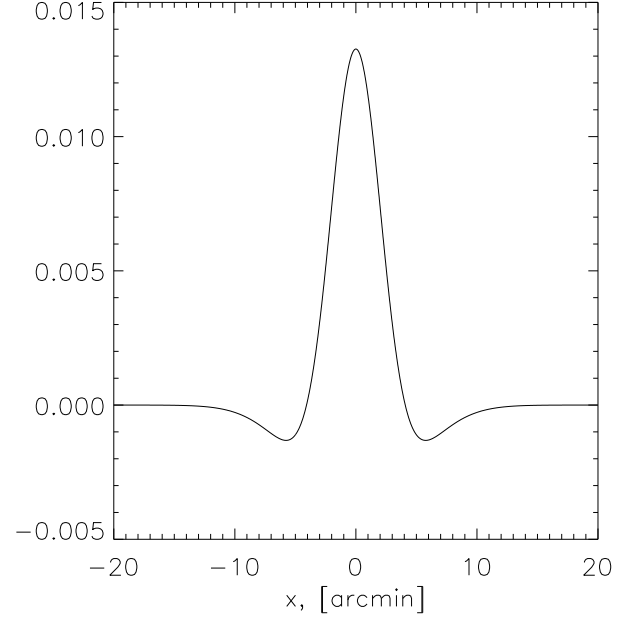
The following formulae demonstrate our convolution procedure. First, we obtain the distribution of stars on the sky M(ra, dec):

$$M(ra, dec) = \sum_i \delta(ra, dec)$$

Then, this map is convolved with the filter:

$$M(ra, dec) = M(ra, dec) * (G(ra, dec, \sigma_1) - G(ra, dec, \sigma_2))$$

where $G(ra, dec, \sigma)$ is the circular 2D Gaussian with unity integral and width of σ. On the last step, we normalize the convolved

Fig. 1. The one-dimensional slice of the 2D filter which we used for the convolution for $\sigma_1 = 3'$ and $\sigma_2 = 6'$
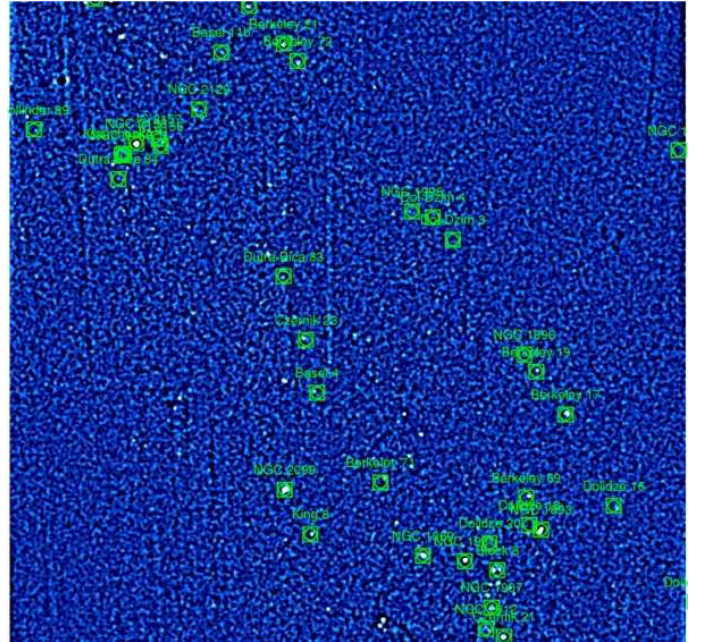
Fig. 2. The $16° \times 16°$ map of the overdensities in the anticenter region from 2MASS PSC. The known open clusters from the Dias catalog (Dias et al., 2002) are marked.

map to get the statistical significances of all density fluctuations:

$$S(ra, dec) = \sqrt{4\pi}\sigma_1 \frac{M(ra, dec) * (G(ra, dec, \sigma_1) - G(ra, dec, \sigma_2))}{\sqrt{M(ra, dec) * G(ra, dec, \sigma_2))}}$$

That map S(ra,dec) shows the deviation of $M(ra, dec) * G(ra, dec, \sigma_1)$ above the background estimate given by $M(ra, dec) * G(ra, dec, \sigma_2)$. Under the assumption of Poisson distribution of sources and $\sigma_2 \gg \sigma_1$, the S(ra,dec) should be normally distributed with variance of 1. The detection of overdensities on this map is very easy and may be done by simple

thresholding, i.e., to select all the overdensities more statistically significant than 5σ, we need find all the pixels on the map having $S(ra, dec) > 5$. We typically used the detection threshold of 4.5 sigmas.

Note that for clusters of the size close to that of the inner Gaussian, the filter is very close to optimal. Also, it is important to understand that the choice of σ_2 is related to the scale on which the background estimate is obtained. Ideally, σ_2 should be rather large and much larger than the σ_1, but unfortunately the 2MASS data in the MW plane suffers significantly from extinction and the density of stars varies on very small scales. Therefore, we are forced to use the σ_2, which is not much larger than σ_1, to have a more local estimate of the background. See also Koposov et al. (2008) for a discussion of the method.

The example of the convolved image from the 2MASS point source catalog for the $16° \times 16°$ anticenter region of our Galaxy is shown in Fig. 2. A large population of peaks is clearly seen. As we show below, most of these peaks can be attributed to open clusters.

After the density peaks are detected, each individual peak should be examined as to whether it relates to a real cluster or just a random fluctuation. To answer this question, we built the Hess-diagram representing the spatial density of stars on a color-magnitude diagram (CMD) (The Hess-diagrams used here are actually the difference of the 2D histogram of color-magnitude of stars inside the circle around the overdensity center (cluster) and the 2D histogram of color-magnitude of stars in the annulus outside the circle (field)). As rule, a real cluster is seen on this Hess-diagram by its main sequence and sometimes, by a red giant branch. If we detected cluster on the Hess-diagram, we fitted its CMD with the isochrone of solar metallicity taken from Girardi et al. (2002). To do this, we automatically shifted the isochrone along the coordinate axes with steps equal to 1/100 of the full range of ordinates and abscissas. At every step, we varied the isochrone age in the interval of $log(age)$ from 6.60 to 10.25 with the step of 0.05. At each step, for each isochrone age, we automatically built the radial density distribution for stars lying in the vicinity of the isochrone (the distance in the color index is less than 0.05 - assumed cluster members) and for all other stars (the distance is greater than 0.05 - supposed field stars). Ideally, the distribution function for field stars should be flat whereas the cluster members should feature a noticeable concentration toward the center. In practice, the radial density distribution of field stars shows a weak central concentration because of the number of unresolved binary stars – cluster members fall into this category (see, for example, Fig. 5) – or because of the poor photometry. That is why to qualify the radial density distribution, we calculated the contrast ratio in the following manner: we divided the value of the peak to the mean plateau for each distribution, then we found the ratio of the two values obtained. For example, in Fig. 5 the contrast is $(4.9/1)/(2.7/2) = 3.63$. We believe that the best position of the isochrone on the color-magnitude diagram corresponds to the maximum contrast ratio at radial density distribution. Testing our technique for well-studied open clusters, we found that the contrast ratio should be greater than 2. By fitting the position of the isochrone to obtain the maximum contrast ratio on the density plot, we simultaneously found main physical parameters of a cluster: age, distance, and color excess. If all plots (Hess-diagram, CMD, and the radial density distribution) verified the reality of the cluster, then the overdensity under study was considered to be a real cluster. Thus, we developed a method of an automated search for stellar overdensities and proposed a reliable criterion for verification of these overdensities as star clusters.

## 3. Application of the method to the 2MASS data

The 2MASS survey (Skrutskie et al., 2006) gives us a comprehensive dataset both to search for new open clusters and to test our method: it covers 99.998% of the sky with uniform precise photometry and astrometry in the J (1.25 μ); H (1.65 μ); and K_s (2.16 μ) photometric bands. The global 2MASS sensitivity is 15.8 for J-band; 15.1 for H-band; and 14.3 for K_s at $S/N = 10$. For this reason, we investigated the $(J, J - H)$ color-magnitude diagrams in our work, but also used $(K_s, J - K_s)$ diagrams to confirm found cluster parameters and be sure that the relation $E(J - H)/E(J - K_s)$ agrees with the normal extinction law.

To extract J, H, K_s photometry and astrometry data, we used the Virtual Observatory resource named Sternberg Astronomical Institute Catalogue Access Services (SAI CAS; `http://vo.astronet.ru`), allowing us to access the largest astronomical catalogs (Koposov et al., 2007b). For our purposes, we only selected the stars that have the quality flags better than U in each filter J, H, K_s.

Our primary goal was to detect clusters that have diameters from few to ten arcminutes, so we used $\sigma_1 = 3'$ and $\sigma_2 = 6'$ in the filter function. Other than the richest ones, clusters having diameters more than 15-20 arcminutes do not show as a rule the visual overdensity on the sky. Such extended clusters are usually found by common proper motions or radial velocities.

As a first application, we studied a field of 16 by 16 degrees towards the Galactic anticenter and detected 88 density peaks of $> 4.5 \times \sigma$ significance. We compared these cluster candidates with open clusters listed by Dias et al. (2002) (in practice, we used the online version of Dias' catalog at `http://www.astro.iag.usp.br/~wilton/`); 23 of our significant peaks can be matched to known, optically-visible clusters. Furthermore, we matched 9 density peaks to embedded infrared clusters from the list created by Bica et al. (2003a,b). Dias' catalog contains an additional 15 open clusters in this region, but our method does not detect them. Six of 15 clusters are not reliable clusters: they are not found in the DSS and 2MASS images, three of them are doubtful clusters according to Dias et al. (2002), one such object has no entry in the WEBDA database on open clusters developed by E. Paunzen and J.-C.Mermilliod (`http://www.univie.ac.at/webda/`). Another 5 clusters having diameters ranging from 20 to 60 arcmin according to Dias et al. (2002), are considered to be clusters due to the common pattern of the proper motion of star members, and only 2 clusters among them, NGC 1912 and NGC 2168, exhibit stellar overdensities. The remaining four clusters have density peaks under $4.5 \times \sigma$ significance, and three of them are seen on 2MASS images as weak embedded clusters. These have no available data, except diameters, in Dias' catalog. Because more than half of the known clusters, that are on our list of detected density peaks have unreliable or no parameter measurements, we completed the detailed analysis of all 88 peaks, including known clusters.

We built the Hess-diagram in $(J, J - H)$ coordinates. We plotted CMD within radius r with the value between 2 and 7 arcmin (depending on the cluster size) around the overdensity center, then we subtracted the CMD for field stars built in the ring between the two radii: $3 \times r$ and $4 \times r$. Each CMD was previously normalized to the number of stars and smoothed using a 3-pixel Gaussian. Figure 3 displays the Hess-diagram for the new open cluster Koposov 52 built within the radius of 4 arcmin around the cluster center (left-hand side) and CMD for field stars in the ring around the cluster (right-hand side). The cluster can clearly
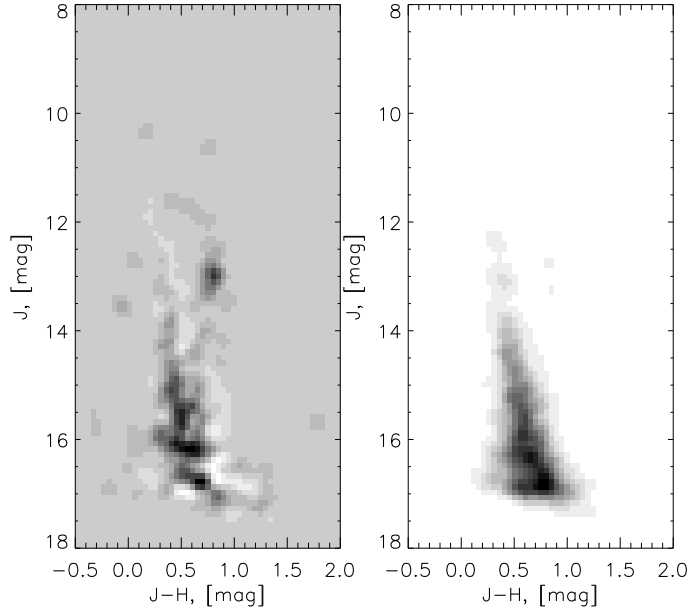
Fig. 3. Hess-diagrams for open cluster Koposov 52. The left panel shows the Hess diagram of the central 4′ of the cluster with subtracted Hess diagram of the background. The right panel shows the Hess diagram of the background stars.

be seen on the Hess-diagram by its main sequence and red clump stars.

If a cluster-suspect manifested itself at the Hess-diagram, then we fitted its CMD with an isochrone, by Girardi et al. (2002) of solar metallicity and simultaneously verified whether the detected stellar group was a real star cluster by plotting radial density distribution for stars lying on the isochrone and for all other stars (see for details Sect. 2). The fitted isochrone with the age of $log(t) = 8.95$ for Koposov 52 is shown in Fig. 4. Star members are taken within the radius of 2 arcmin around its center; the position of the isochrone leads to the following estimations: $E(J - H) = 0.34$ and $(m - M)_J = 13.20$. The radial density distribution corresponding to this fitted isochrone is displayed in Fig. 5: solid circles denote the stars deviating from the isochrone by less than 0.05 magnitude in color $(J - H)$; open circles denote all other stars. Therefore, the total density profile of all stars is the sum of the open circle profile and solid circle profile. The errors plotted on the datapoints are simple Poisson errors. The ratio of contrasts for the "isochrone" and "field" stars calculated in Sect. 2 equals to 3.63. It is important to note that the background value (value at large radii) for the solid circle profile is much lower than the background value for the empty circle profile. This illustrates the advantage of using the isochrone filter for the detection and analysis of overdensities – with such a filter, overdensity is much more obvious due to the reduced background.

We performed isochrone fitting on $(J, J - H)$ diagram because there is a higher magnitude limit for J-band in 2MASS, and used a 15-arcmin region around stellar overdensity. We independently performed the same fitting procedure on a $(K_s, J - K_s)$ CMD and compared the distances obtained from two fittings with each other, and the relation $E(J-H)/E(J-K_s)$ with the normal extinction law given by Cardelli et al. (1989), which equals to 0.55. Also we used the relations $A_{K_s} = 0.670 \times E(J-K_s)$,
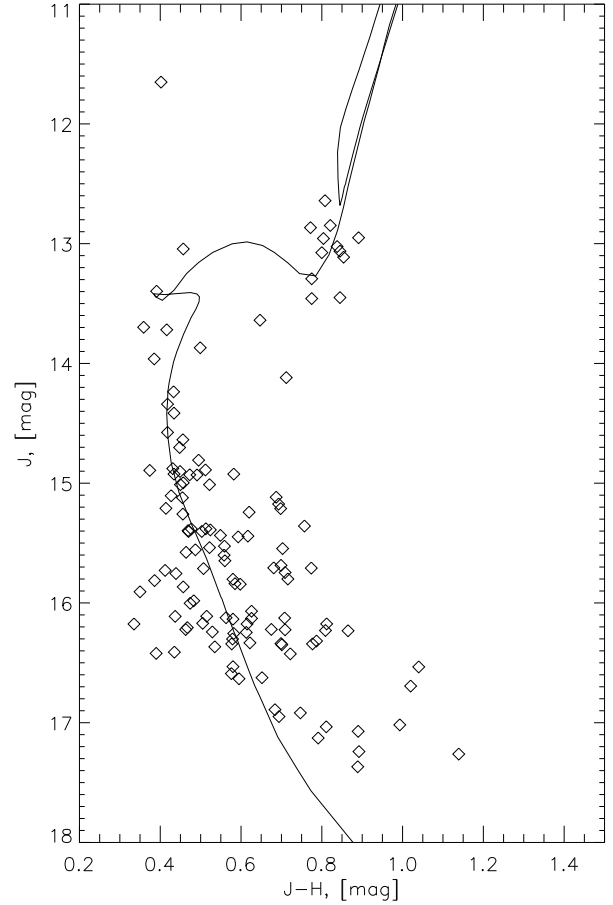
Fig. 4. Color-magnitude diagram for cluster Koposov 52 inside the radius of 2 arcminutes. The fitted isochrone with $log(t) = 8.95$, $E(B - V) = 0.04$, $(m - M)_0 = 12.32$ is overplotted.

$A_J = 0.276 \times A_V$, and $E(J - H) = 0.33 \times E(B - V)$ from the paper by Dutra et al. (2002).
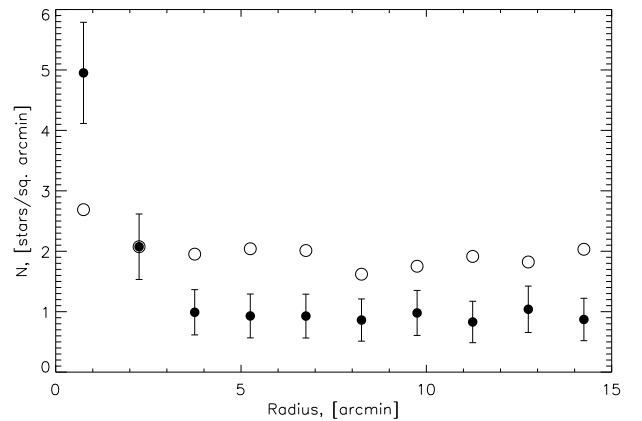
Fig. 5. Radial density distribution for stars in the field of Koposov 52. Solid circles represent the density of the stars lying closely to the isochrone. Open circles denote the density of the field stars lying far from the isochrone.

Table 2. Coordinates of new infrared embedded clusters

Name	Other name	RA (J2000) h:m:s	Dec (J2000) d:m:s	D arcmin
Koposov 7	FSR 784	05:40:44.1	+35:55:25	6
Koposov 41	FSR 839	06:03:58.0	+30:15:41	4
Koposov 58	FSR 849	05:51:11.0	+25:46:41	2
Koposov 82	Teutsch 136	06:11:55.8	+20:40:14	4

The cluster was considered to be a real cluster, if all plots (Hess-diagram, CMD, and the radial density distribution) verified the reality of the cluster.

4. Results

We used the routine described above to study all 88 overdensities. We found that 11 stellar overdensities turn out to be new, optically-visible clusters. The parameters for all these clusters are listed in Table 1. One of them, Koposov 52, was published earlier as KSE18 (Koposov et al., 2005; Zolotukhin et al., 2006) and then independently found by Kronberger et al. (2006) as Teutsch 51. Four other clusters coincide with cluster candidates from the list compiled by Froebrich et al. (2007), and two clusters coincide with stellar agglomerations reported by Kronberger et al. (2006). Note that in both papers cited, these objects are considered as possible clusters with futher investigation necessary to clarify their nature. In our work, we not only discovered these clusters by an independent method, but also verified their nature and found their fundamental parameters. That is why we consider them as new clusters.

Note that we are not able to make a precise estimation of the age of the young clusters, if their color-magnitude diagrams do not exhibit red or blue giants or supergiants. Provided that the positions of an isochrone with respect to the axes of coordinates is unchanged, we can alter its age within a broad range (in some cases, up to 8.20 in $log(age)$) without having a noticeable effect on the contrast on the radial-density distribution plot. This can be attributed to the existence of an extended vertical section of $(J, J − H)$ and $(K_s, J − K_s)$ isochrones and the absence of massive stars in poor clusters. Therefore, we were only able to make the upper boundary for the age estimation of Koposov 36 and Koposov 53, Koposov 10, Koposov 27, and Koposov 49 clusters. While it is possible that some of the bright stars on the CMD are giants belonging the cluster, there is no statistically meaningful way to check that with only photometric data, therefore we assign only the upper limits for the ages of these 5 clusters.

The errors in color excess, distance moduli, distances and ages are evaluated from the differences in the parameters derived from isochrones fitted in $(J, J − H)$ and $(K_s, J − K_s)$ diagrams. Hess-diagrams, radial density distribution, and fitted isochrone in $(J, J−H)$ CMD's for 10 new clusters (except for Koposov 52) are given in Fig.7-16 in the Appendix. Four of the 11 new clusters are relatively young, less than 100 Myr, whereas the other clusters in this set are very old, exceeding 1 Gyr. Distances of all clusters from the Sun are ranged between 1.5 and 3.5 kpc.

Also, we found 4 new infrared clusters embedded in the nebulae, which are similar to the clusters found by Bica et al. (2003a) and Bica et al. (2003b): their coordinates are presented in Table 2, and Hess-diagrams are shown in Fig.17-18 in the Appendix. For IR clusters, the cluster reveals itself as a cloud on the left-hand diagram; the effect of the differential extinction is also clearly noticeable. The right-hand diagram displays CMD of field stars around the cluster. Because of a high value
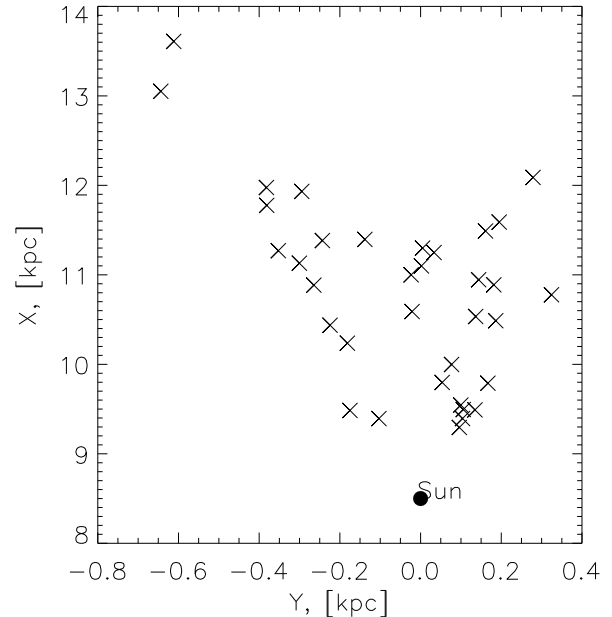
Fig. 6. Distribution of clusters across the galactic plane.

of reddening, it was impossible to fit isochrones and find parameters for these clusters, except Koposov 41. The Hess-diagram for this cluster exhibits the main sequence, and we can fit it with the isochrone of the age of 4 Myr. This best-fit isochrone was used to find the distance of 2200 pc and the color excess of $E(B − V) = 1.95$.

Thirty two overdensities turned out to be known clusters: 23 were matched to the objects from the Dias catalog (Dias et al., 2002), and 9, to IR clusters from the list by Bica et al. (2003a) and Bica et al. (2003b).

In Table 3, we present the data for all clusters from the catalog compiled by Dias et al. (2002), that were detected by our technique within the square region studied. Although two clusters, NGC 1912 and NGC 2168, were not detected because of their large diameters (about 25 arcmin), we added their parameters to the table, as they exhibit slight overdensities and can be studied by our methods. In some cases, we obtained more precise coordinates of the center of clusters, so we give new coordinates for all clusters.

In the columns, we give parameters of the clusters both listed in the Dias catalog (Dias et al., 2002) or in WEBDA database and measured by applying our methodology to the 2MASS catalog. For clusters Be 72, Cz 21, Cz 23, Cz 24, DC 8, Pis 27, Dias does not publish any parameters except their coordinates and diameters. However, in the WEBDA database there are data on Be 71 taken from the paper by Lata et al. (2004): $E(B − V) = 0.85$, $d = 3900 pc$, $log(t) = 8.80$. We observe that the color excess and the age well agree with our parameters, whereas the distance exceeds our value by 1500 pc. The difference in distance evaluations (when the age estimations are pretty close) can be attributed to the fact that the authors fitted $(V, B − V)$ CMD by Zero Age Main Sequence (ZAMS) given by Schmidt-Kaler (1982) to estimate the distance modulus, and the theoretical isochrones given by Girardi et al. (2002) to find the cluster's age, while we used 2MASS theoretical isochrones by Girardi et al. (2002) to evaluate all cluster's parameters.

Table 1. Parameters of new clusters

Name	Other name	RA (J2000)	Dec (J2000)	D	E(B-V)	$\frac{E(J-H)}{E(J-K)}$	$(m-M)_0$	Distance	Age
		h:m:s	d:m:s	arcmin	mag		mag	pc	log(yr)
Koposov 10	FSR 795	05:47:28.6	+35:25:56	4	0.81±0.25	0.79	11.54±0.3	2000±300	<8.6
Koposov 12	FSR 802	06:00:56.2	+35:16:36	9	0.30±0.03	0.51	11.55±0.03	2050±50	8.90±0.1
Koposov 27	Teutsch 1	05:39:30.0	+33:21:00	3	0.45±0.1	0.69	12.8±0.5	3700±900	<8.65
Koposov 36		05:36:50.6	+31:12:39	9	0.83±0.11	0.63	11.16±0.16	1700±150	<8.35
Koposov 43	FSR 848	05:52:14.6	+29:55:09	8	0.38±0.10	0.44	12.21±0.09	2800±120	9.30±0.1
Koposov 49	Teutsch 10	05:44:22.2	+28:49:13	6	0.42±0.05	0.94	11.46±0.22	2000±200	<9.15
Koposov 52	Teutsch 5	05:53:48.9	+26:50:26	5	1.03±0.04	0.58	12.32±0.11	2900±140	8.95±0.1
Koposov 53		06:08:56.2	+26:15:49	3	0.34±0.04	0.61	12.52±0.03	3200±100	<8.5
Koposov 62		06:18:02.0	+24:42:38	6	0.34±0.02	0.57	12.21±0.05	2800±60	9.40±0.1
Koposov 63	FSR 869	06:10:01.7	+24:33:38	5	0.26±0.04	0.40	12.32±0.28	3000±350	9.15±0.1
Koposov 77		05:43:52.3	+21:42:37	5	0.57±0.01	0.55	11.23±0.02	1750±50	9.65±0.1
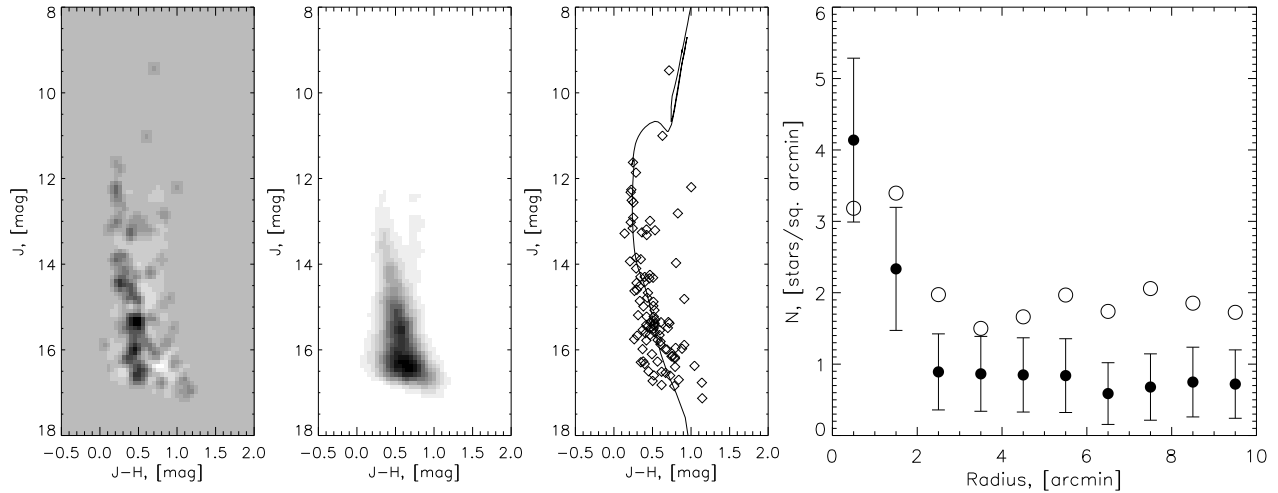
Fig. 7. First and second columns: Hess diagram of the Koposov 10 cluster and Hess diagram of the background. Third column: CMD diagram of the stars within 2′ from the center of the Koposov 10 with the fitted isochrone. Fourth column: Radial density distribution for Koposov 10, the symbols used are the same as in Fig. 5.

Parameters we measured for 7 clusters (Be 19, Be 71, Kronberger 1, King 8, NGC 1931, Stock 8 and NGC 2158) significantly differ from the data in the catalog by Dias et al. (2002) and in WEBDA, but we suppose our results are more precise and homogeneous. Parameters of Be 19 were obtained by Christian (1980) as following: employing the UBV photographic photometry data, the author compared the CMD of Be 19 with both the color-magnitude diagram of NGC 752 and the theoretical isochrones by Ciardullo (1979). Parameters of King 8 cluster, which appeared in the catalog by Dias et al. (2002) were calculated by Loktin et al. (2001) using photographic photometry by Christian (1981). However, Christian (1981) published the distance to the clusters equal to 3.5 kpc, which essentially differs from the value of 6403 pc by Loktin et al. (2001). Parameters of Stock 8 were also obtained by Loktin et al. (2001) using the UBV photometry of 32 stars only measured by different authors; these stars do not show any sequence on CMD. As for cluster Kronberger 1, the isochrone corresponding to the parameters available in the Dias et al. (2002) catalog fitted the main sequence of field stars, whereas the cluster members are noticeably shifted to the right in the $(J, J - H)$ CMD because of extinction. The effect of extinction is clearly seen on the corresponding Hess-diagrams. Parameters of NGC 1931 cluster were obtained by Loktin et al. (2001) using published photometry data by Bhatt et al. (1994), but the authors themselves

give the distance of 2170 pc. This cluster is embedded in a nebula, so its Hess-diagram shows a slightly scattered area occupied by the cluster. We fitted its CMD with a very young isochrone, and the distance appeared to be three times smaller than that by Dias et al. (2002). The estimations of the distance to NGC 2158 cluster differ from each other very noticeably (by 2 kpc). Dias et al. (2002) take data from Loktin et al. (2001), who used compilative data and automatic method to find the cluster's parameters. At the same time, our data are in good accordance with parameters by Carraro et al. (2002) who obtained 3600 pc for the distance, $E(B - V) = 0.55$, and $log(t) = 9.3$ by fitting isochrone from Girardi et al. (2000) and then comparing the best-fit with the simulated synthetic CMD. The discussion above demonstrates that the authors often publish controversial estimations of the cluster parameters even if they employ the same observational data. Although our estimations are sometimes based on less deep photometric data, they have an essential advantage in homogeneity of both observational data and used isochrones and fitting methods.

Members of NGC 1893 cluster detected on the Hess-diagram do not lie on the same isochrone, so we cannot find a satisfactory fitting. This fact can be reasonably attributed to the existence of pre-main sequence stars in this cluster described by Vallenari et al. (1999). The distance to the cluster found by
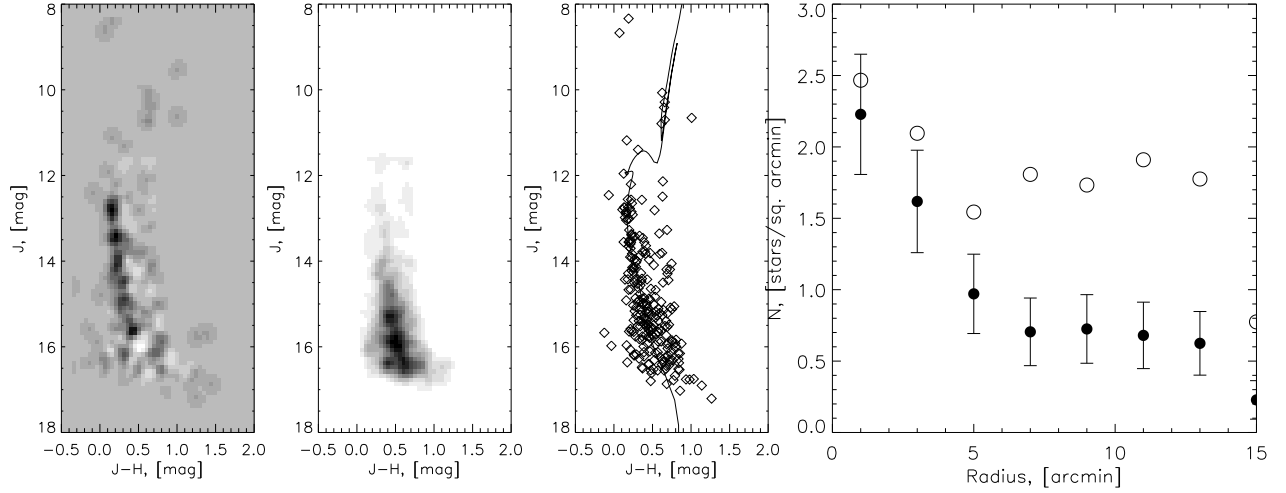
Fig. 8. First and second columns: Hess diagram of the Koposov 12 cluster and Hess diagram of the background. Third column: CMD diagram of the stars within $4'$ from the center of the Koposov 12 with the fitted isochrone. Fourth column: Radial density distribution for Koposov 12, the symbols used are the same as in Fig. 5.
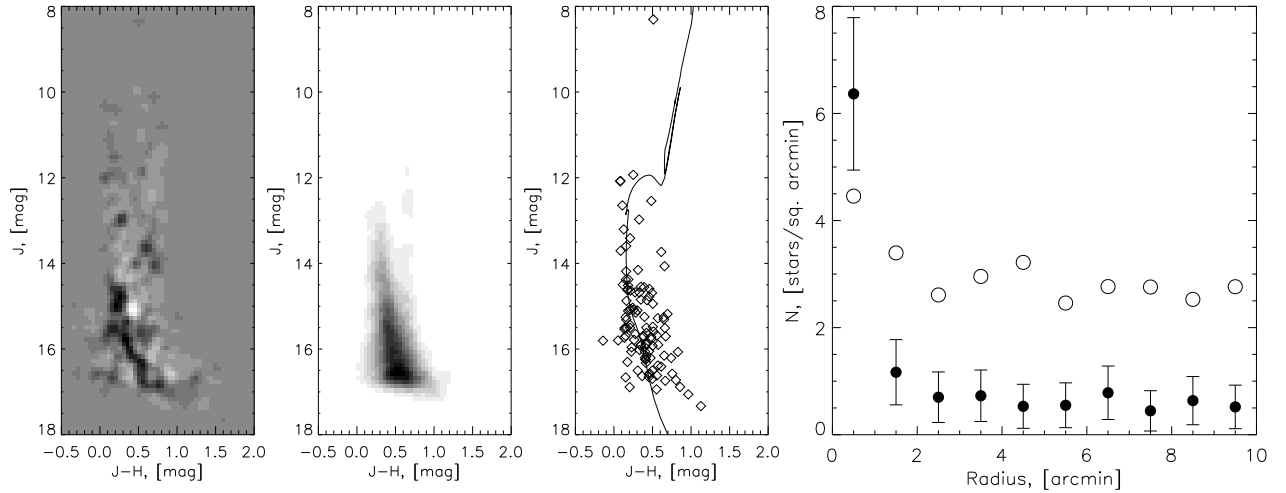
Fig. 9. First and second columns: Hess diagram of the Koposov 27 cluster and Hess diagram of the background. Third column: CMD diagram of the stars within $2'$ from the center of the Koposov 27 with the fitted isochrone. Fourth column: Radial density distribution for Koposov 27, the symbols used are the same as in Fig. 5.

Vallenari et al. (1999) equals 4300 pc (cf. with 6000 pc in the Dias catalog).

In the remaining 11 cases, our parameters closely agree (to within the error levels) with the corresponding data available from the catalog by Dias et al. (2002). These error levels are as follow: 200-500 pc for the distances, 0.10^m for the color excess $E(B - V)$, and 0.05 for $log(t)$.

There are five additional clusters that have parameters in Dias' catalog and that were not detected in the field under study (see Sect. 3). However, the distances and other parameters for four of them were obtained from very poor (V,B-V) diagrams, which do not show any sequence or clump at the CMD, and we did not consider these clusters.

At the end, 41 of 88 density peaks showed no evidence of being real clusters. In these cases, we detect either a nebula, or a bright star, or occasional groups of stars, whose density for some reasons exceeds the density of field stars.

In Fig. 6, we also show the distribution of all clusters under investigation across the galactic plane: both the newly-opened clusters and the known ones, whose parameters were (re)determined in the present study. The crosses indicate the clusters with $log(age)$ less then 8.00; all young clusters are situated from 1 to 3.5 kpc from the Sun.

We do not quantify the detection efficiency of our algorithm. In the square under our study in the vicinity of the Galactic anticenter, we detect as much as 95% of clusters listed with the diameters less than 15 arcminutes in the Dias et al. (2002) catalog. But ideally the efficiency can be determined only with simulations, since none of existing catalags is complete and free of selection effects. The detailed analysis of the detection efficiency and selection effects of the algorithm is left for our future work.
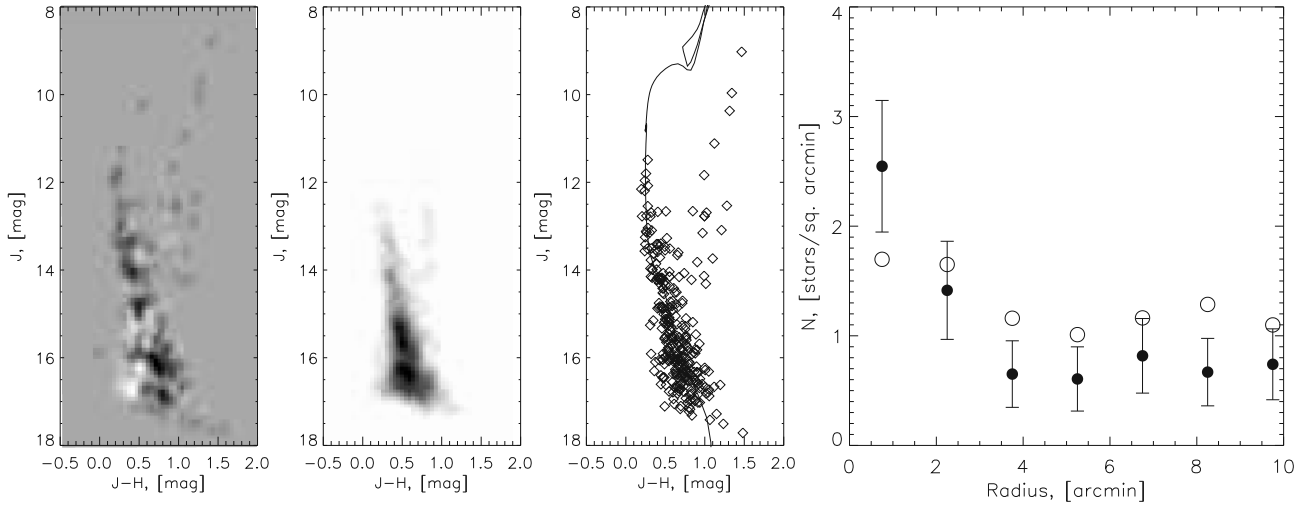
Fig. 10. First and second columns: Hess diagram of the Koposov 36 cluster and Hess diagram of the background. Third column: CMD diagram of the stars within 4′ from the center of the Koposov 36 with the fitted isochrone. Fourth column: Radial density distribution for Koposov 36, the symbols used are the same as in Fig. 5.
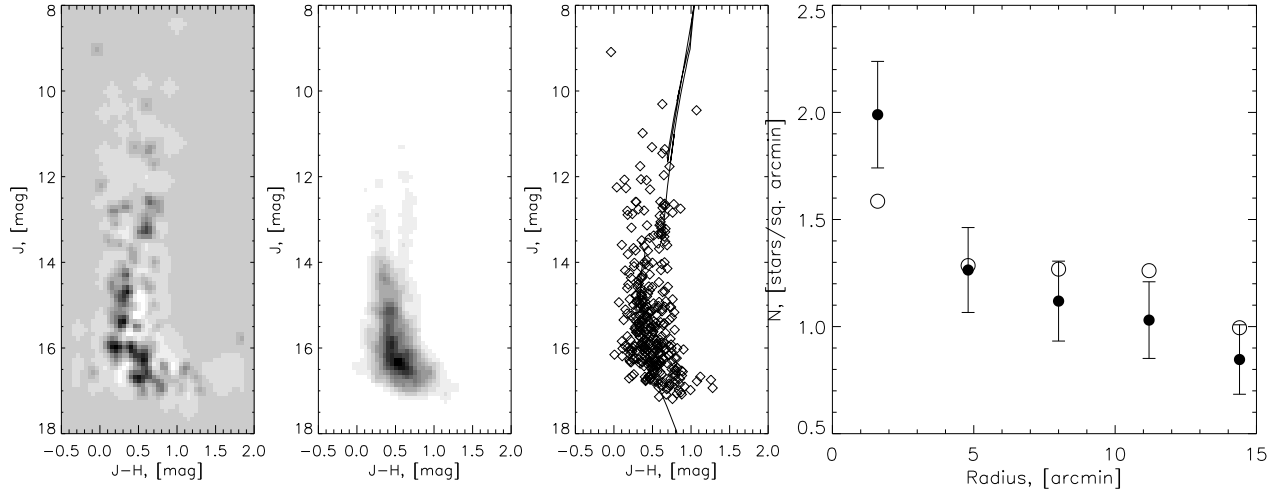
Fig. 11. First and second columns: Hess diagram of the Koposov 43 cluster and Hess diagram of the background. Third column: CMD diagram of the stars within 4′ from the center of the Koposov 43 with the fitted isochrone. Fourth column: Radial density distribution for Koposov 43, the symbols used are the same as in Fig. 5.

5. Conclusions

We have demonstrated the new method of searching for star clusters in the data from large surveys and applied it to the 2MASS data. In the small field of 16 by 16 degrees in the poor region of Galactic anticenter, we have found and verified 15 new open clusters. Ten of them coincide with cluster candidates from papers by Froebrich et al. (2007) and Kronberger et al. (2006). However, we not only discovered these objects independently, but also investigated their nature. We developed an automated method, which involves three different techniques: Hess-diagram, color-magnitude diagram in $(J, J − H)$ and $(K_s, J − K_s)$, and radial density distribution. For 12 of the new clusters, we obtained main physical parameters: ages, distances, and color excesses. We also used our methods to evaluate the same physical parameters for all known clusters detected in the selected area. We found that out of 25 such clusters, only in 11 cases we can accept the values of the cluster parameters listed in the catalog by Dias et al. (2002). We have found, or improved, the distances,

ages, and color excesses for 13 previously-known clusters. As one can see from Fig. 6, the number of clusters in the square studied, for which their main physical parameters are reliably evaluated, has increased from 11 in the catalog by Dias et al. (2002) to 35 in our study.

Therefore, to get a catalog of homogeneously-measured parameters of open clusters, it is necessary not only to search for new clusters and thoroughly investigate them, but also to recalculate the parameters of all known clusters using uniform raw datasets and a uniform and automated processing methodology.
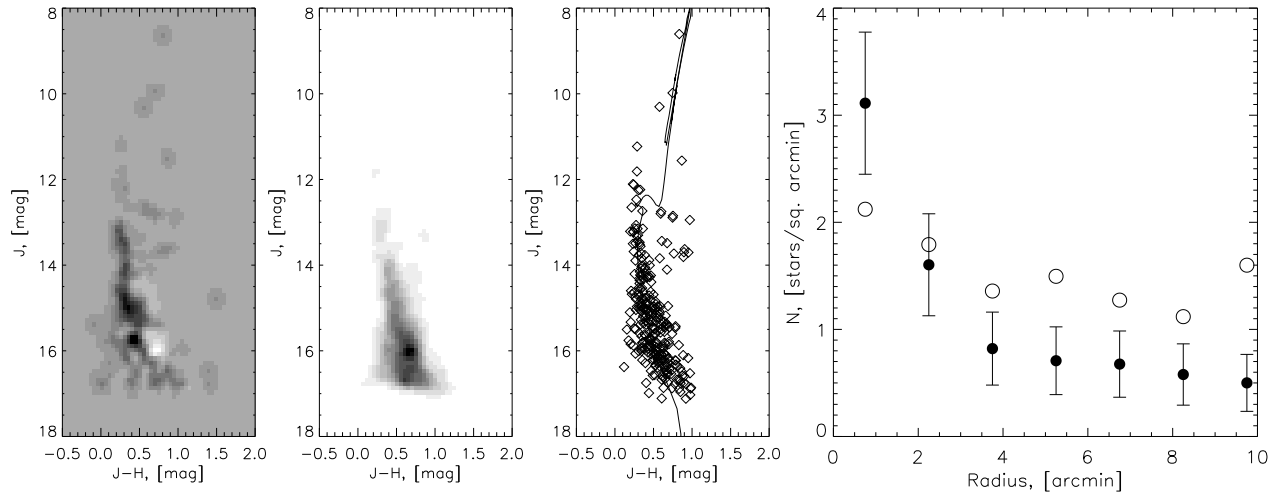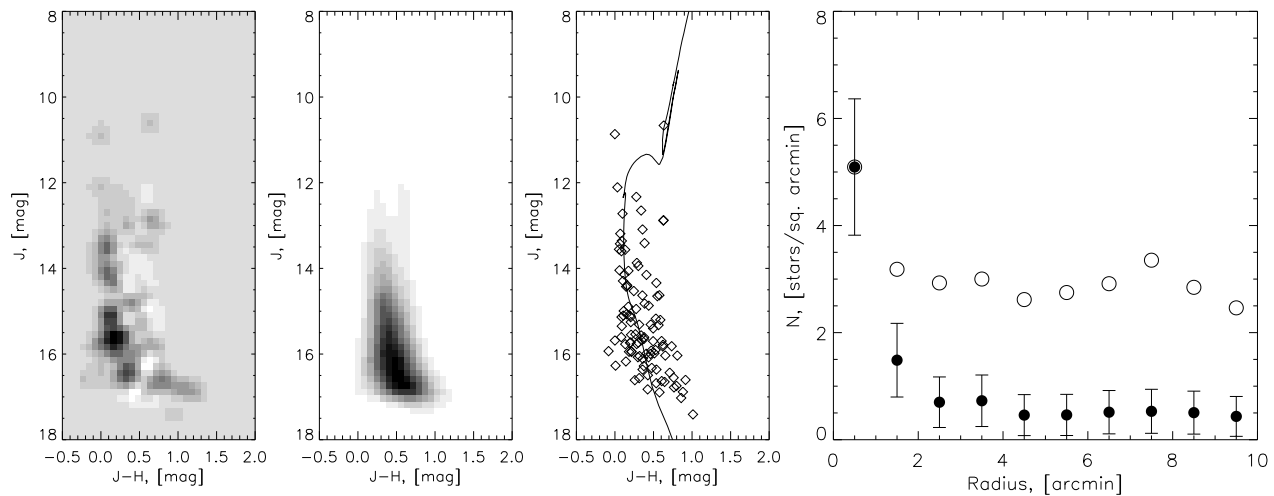
Fig. 12. First and second columns: Hess diagram of the Koposov 49 cluster and Hess diagram of the background. Third column: CMD diagram of the stars within 4′ from the center of the Koposov 49 with the fitted isochrone. Fourth column: Radial density distribution for Koposov 49, the symbols used are the same as in Fig. 5.
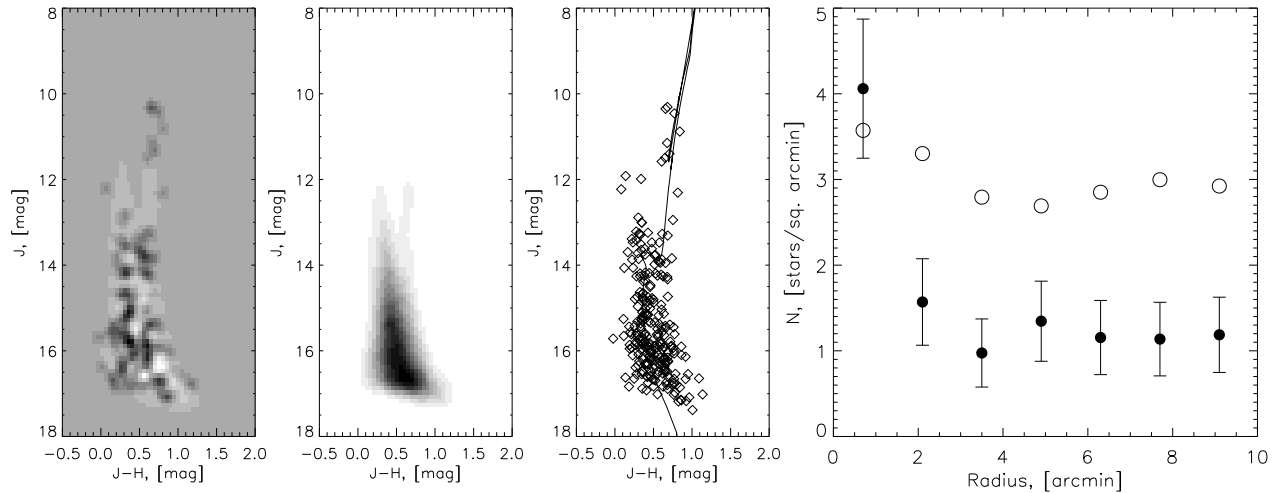

Fig. 13. First and second columns: Hess diagram of the Koposov 53 cluster and Hess diagram of the background. Third column: CMD diagram of the stars within 4′ from the center of the Koposov 53 with the fitted isochrone. Fourth column: Radial density distribution for Koposov 53, the symbols used are the same as in Fig. 5.

References

Babaud J., A. P. Witkin, M. Baudin, and R. O. Duda. 1986, IEEE Trans. Pattern Anal. Mach. Intell., 8, 1, 26
Bica, E., Dutra, C. M., Soares, J., & Barbuy, B. 2003a, A&A, 404, 223
Bica, E., Dutra, C. M., & Barbuy, B. 2003b, A&A, 397, 177
Bhatt, B. C., Pandey, A. K., Mahra, H. S., & Paliwal, D. C. 1994, Bulletin of the Astronomical Society of India, 22, 291
Borissova, J., Pessev, P., Ivanov, V. D., Saviane, I., Kurtev, R., & Ivanov, G. R. 2003, A&A, 411, 83
Cardelli, J. A., Clayton, G. C., & Mathis, J. S. 1989, ApJ, 345, 245
Carraro, G., Girardi, L., & Marigo, P. 2002, MNRAS, 332, 705
Ciardullo, R. B., & Demarque, P. 1979, In "Problems of Calibration of Multicolor Photometric Systems," Dudley Observatory 14, 317
Christian, C. A. 1980, AJ, 85, 700
Christian, C. A. 1981, ApJ, 246, 827
Dias, W. S., Alessi, B. S., Moitinho, A., & Lépine, J. R. D. 2002, A&A, 389, 871 and online version www.astro.iag.usp.br/ wilton/clusters.txt
Drake, A. J. 2005, A&A, 435, 545
Dutra, C. M., Santiago, B. X., & Bica, E. 2002, A&A, 381, 219
Dutra, C. M., Bica, E., Soares, J., & Barbuy, B. 2003, A&A, 400, 533
Froebrich, D., Scholz, A., Raftery, C. L. 2007, MNRAS, 374, 399
Girardi, L., Bressan, A., Bertelli, G., & Chiosi, C. 2000, A&AS, 141, 371
Girardi, L., Bertelli, G., Bressan, A., Chiosi, C., Groenewegen, M. A. T., Marigo, P., Salasnich, B., & Weiss, A. 2002, A&A, 391, 195
Ivanov, V. D., Borissova, J., Pessev, P., Ivanov, G. R., & Kurtev, R. 2002, A&A, 394, L1
Koposov, S., Glushkova, E., & Zolotukhin, I. 2005, Astronomische Nachrichten, 326, 597
Koposov, S., et al. 2007, ApJ, 669, 337
Koposov, S., et al. 2008, ArXiv e-prints, 706, arXiv:0706.2687, accepted to ApJ
Koposov, S. E., Bartunov, O., & Karpov, S. 2007, Highlights of Astronomy, 14, 586
Kronberger, M., et al. 2006, A&A, 447, 921
Lata, S., Mohan, V., & Sagar, R. 2004, Bulletin of the Astronomical Society of India, 32, 371

Fig. 14. First and second columns: Hess diagram of the Koposov 62 cluster and Hess diagram of the background. Third column: CMD diagram of the stars within 3′ from the center of the Koposov 62 with the fitted isochrone. Fourth column: Radial density distribution for Koposov 62, the symbols used are the same as in Fig. 5.
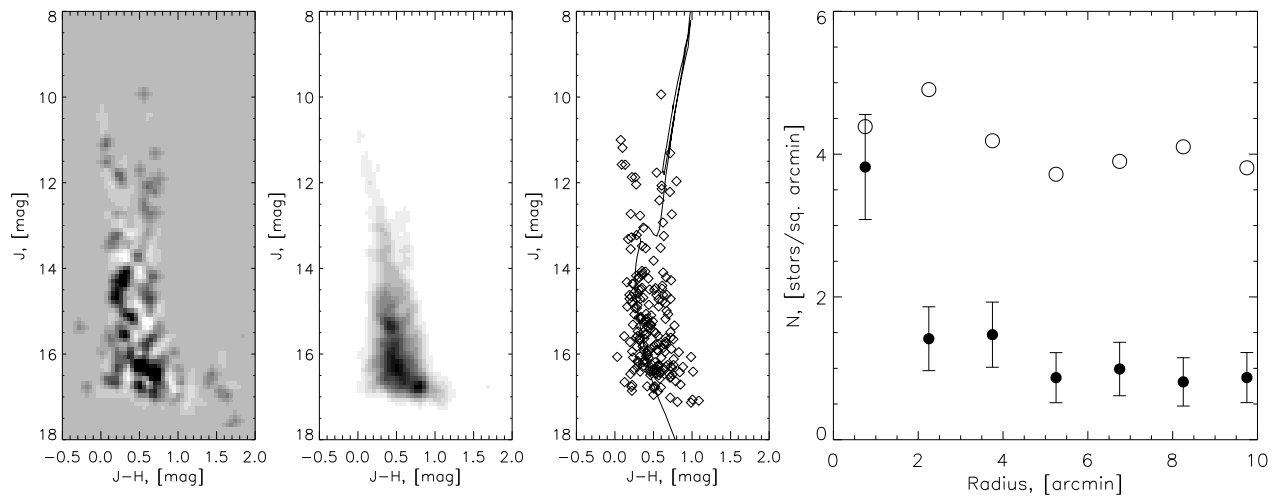
Fig. 15. Koposov 63 open cluster. First and second columns: Hess diagram of the Koposov 63 cluster and Hess diagram of the background. Third column: CMD diagram of the stars within 2′.5 from the center of the Koposov 63 with the fitted isochrone. Fourth column: Radial density distribution for Koposov 63, the symbols used are the same as on figure 5.

Lindenberg, T., 1998, International Journal of Computer Vision, 30, 2, 79

Loktin, A. V., Gerasimenko, T. P., & Malisheva L. K. 2001, Astron. Astrophys. Trans. 20, 607

Paunzen E., Mermilliod J.-C. http://www.univie.ac.at/webda/

Schmidt-Kaler Th. 1982, in Scaifers K., Voigt H. H., eds, Landolt/Bornstein, Numerical Data and Functional Relationship in Science and Technology, New series, Group VI, Vol. 2b. Springer-Verlag, Berlin, Pp. 14.

Skrutskie, M. F., et al. 2006, AJ, 131, 1163

Surdin, V. G. 2000, Formación estelar, Editorial URSS, Moscú, 272p.

Vallenari, A., Richichi, A., Carraro, G., & Girardi, L. 1999, A&A, 349, 825

Zolotukhin, I., Koposov, S., & Glushkova, E. 2006, ASP Conf. Ser. 351: Astronomical Data Analysis Software and Systems XV, 351, 240
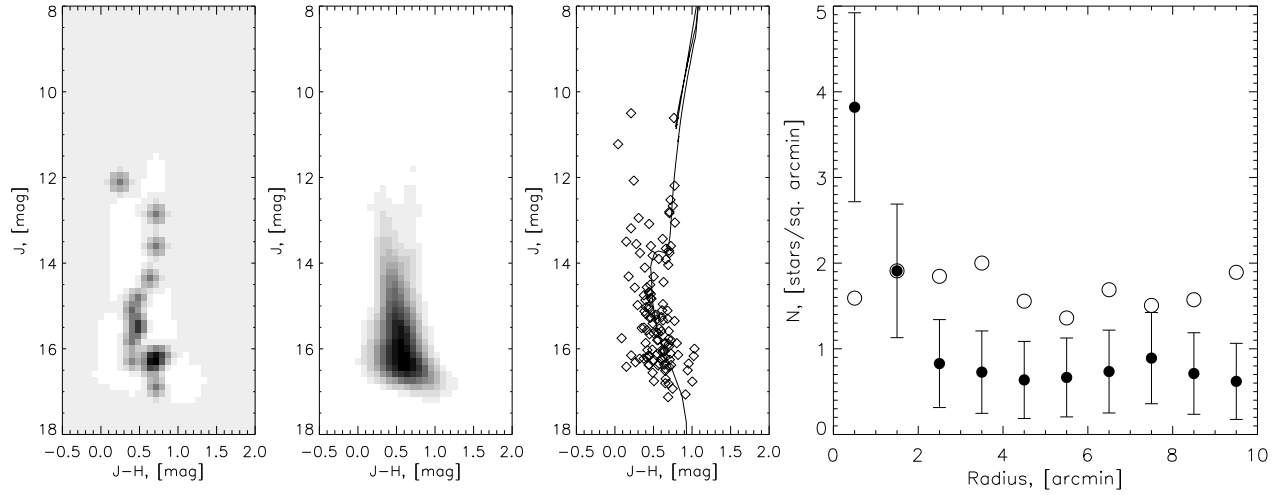
Fig. 16. Koposov 77 open cluster. First and second columns: Hess diagram of the Koposov 77 cluster and Hess diagram of the background. Third column: CMD diagram of the stars within $2'.5$ from the center of the Koposov 77 with the fitted isochrone. Fourth column: Radial density distribution for Koposov 77, the symbols used are the same as on figure 5.
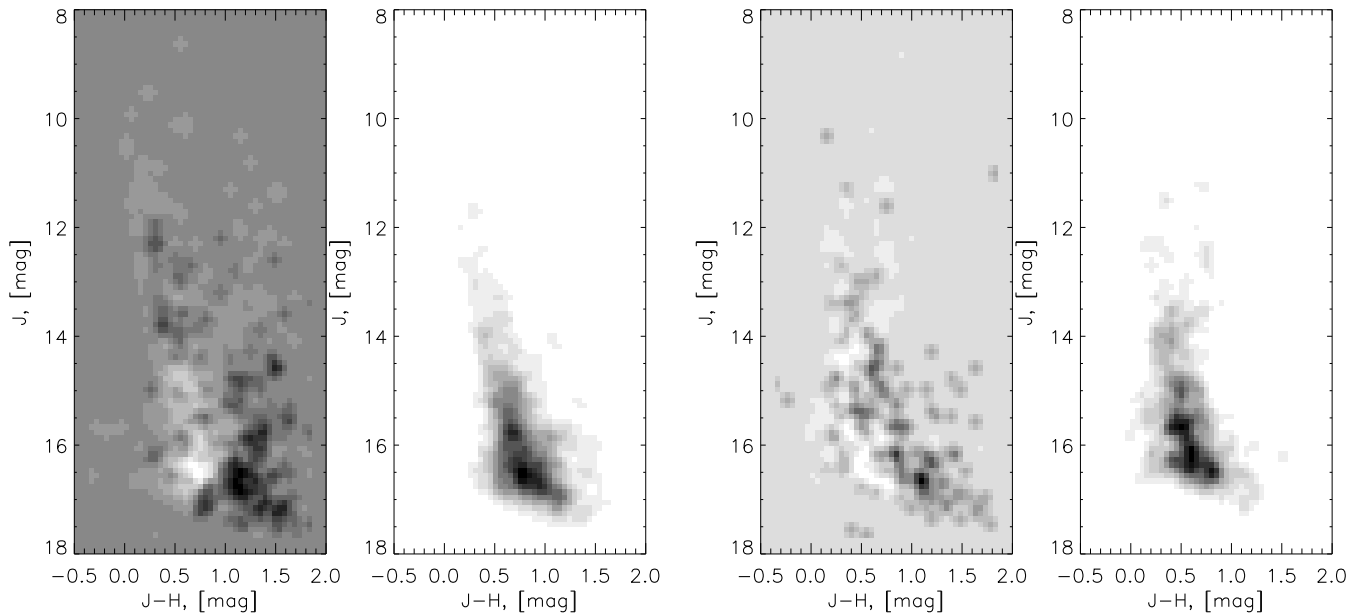
Fig. 17. Left panel: Hess diagram of the IR-embedded cluster Koposov 7 and Hess diagram of the background. Right panel: Hess diagram of the IR-embedded cluster Koposov 41 and Hess diagram of the background
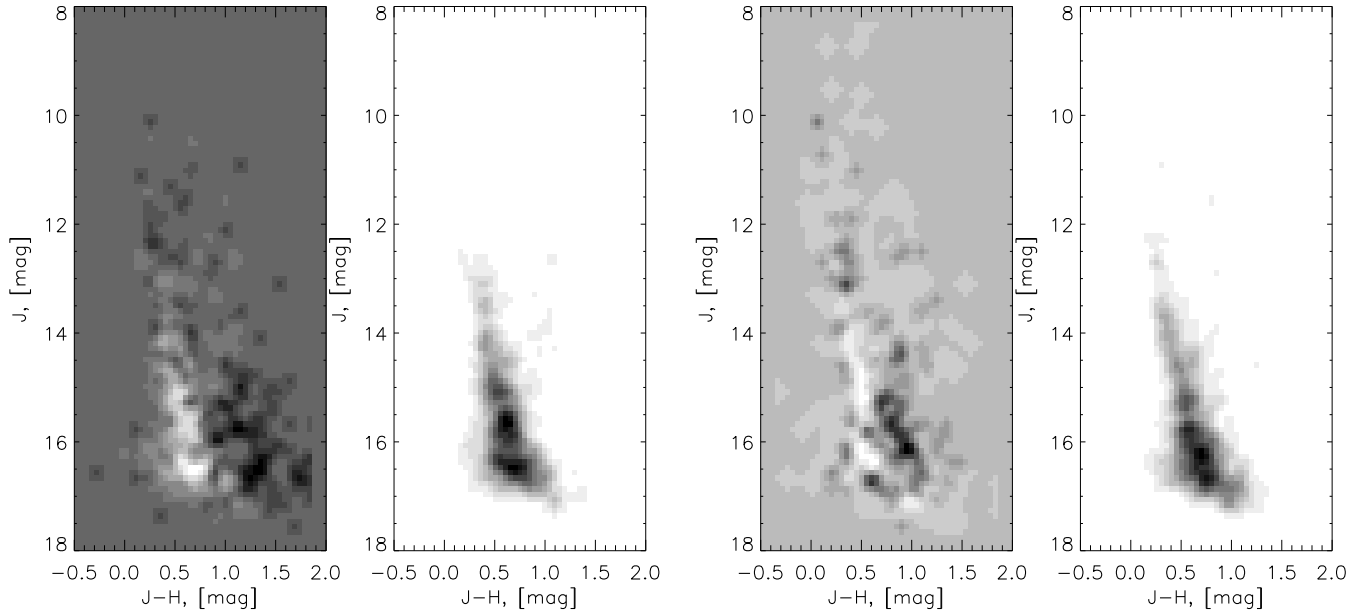
Fig. 18. Left panel: Hess diagram of the IR-embedded cluster Koposov 58 and Hess diagram of the background. Right panel: Hess diagram of the IR-embedded cluster Koposov 82 and Hess diagram of the background

Table 3. Comparison of physical parameters of the clusters: Dias catalog and Paunzen-Mermilliod database (DPM) vs. present study (KGZ)

Name	RA(J2000) h:m:s	Dec(J2000) d:m:s	D_{DPM} pc	D_{KGZ} pc	$E(B-V)_{DPM}$ mag	$E(B-V)_{KGZ}$ mag	Age_{DPM} log(yr)	Age_{KGZ} log(yr)
Basel 4	05:48:54.9	+30:11:08	3000	2750	0.45	0.57	8.30	8.25
Berkeley 17	05:20:29.6	+30:34:33	2700	2400	0.58	0.30	10.00	10.00
Berkeley 19	05:24:02.8	+29:34:16	4831	3000	0.40	0.61	9.49	9.25
Berkeley 21	05:51:47.4	+21:48:31	5000	5150	0.76	0.51	9.34	9.35
Berkeley 69	05:42:22.6	+22:50:01	2860	2900	0.65	0.45	8.95	9.00
Berkeley 71	05:40:56.7	+32:16:33	3900	2450	0.85	0.91	8.80	8.80
Berkeley 72	05:50:17.6	+22:14:59		3500		0.43		8.65
Czernik 21	05:26:41.0	+36:00:49		2300		0.72		9.55
Czernik 23	05:50:03.6	+28:53:41		2500		0.38		8.45
Czernik 24	05:55:24.6	+20:53:11		4600		0.26		9.40
DC 8	06:09:21.3	+31:13:54		2100		0.72		9.00
IC 2157	06:04:41.9	+24:06:01	2040	2400	0.548	0.58	7.800	<7.6
King 8	05:49:19.0	+33:37:38	6403	3100	0.580	0.44	8.618	9.05
Kronberger 1	05:28:22.0	+34:46:24	1900	800	0.52	0.43	7.5	8.10
NGC 1893	05:22:53.7	+33:26:17	6000		0.45		6.48	
NGC 1907	05:28:10.7	+35:19:44	1800	1300	0.52	0.51	8.5	8.60
NGC 1931	05:31:25.9	+34:12:50	3086	1000	0.738	1.97	7.002	<7.0
NGC 1960	05:36:19.6	+34:07:27	1330	1050	0.22	0.19	7.4	<7.5
NGC 2099	05:52:18.4	+32:33:03	1383	1300	0.302	0.27	8.540	8.60
NGC 2129	06:01:10.5	+23:19:34	2200	1950	0.80	0.82	7.00	7.10
NGC 2158	06:07:27.8	+24:05:53	5071	3300	0.360	0.34	9.023	9.30
Pismis 27	06:10:53.8	+20:36:26		1000		0.68		<7.7
Stock 8	05:28:08.8	+34:25:53	1821	900	0.445	1.21	7.056	<7.5
NGC 1912	05:28:41.6	+35:48:34	1400	1000	0.25	0.38	8.5	8.30
NGC 2168	06:09:00.0	+24:21:00	912	900	0.20	0.19	8.25	7.95